Tuning the size of poly(butylene oxide) nanoparticles by microfluidic-assisted nanoprecipitation

Lachlan Alexander, Marat Mamurov, Hiba Khelifa, Nicolas Illy, Philippe Guégan, Christophe M Thomas, Samuel Hidalgo-Caballero, Joshua D Mcgraw, Kawthar Bouchemal

ARTICLE

Tuning the size of poly(butylene oxide) nanoparticles by microfluidic-assisted nanoprecipitation

Received 00th January 20xx,
Accepted 00th January 20xx

DOI: 10.1039/x0xx00000x

Lachlan Alexander,[a,b,c#] Marat Mamurov,[a,c#] Hiba Khelifa,[a,d#] Nicolas Illy,[d] Philippe Guégan,[d] Christophe M. Thomas,[a] Samuel Hidalgo-Caballero,[c,e] Joshua D. McGraw,[c,e*] and Kawthar Bouchemal [a*]

Microfluidic-assisted nanoprecipitation offers precise control over process parameters, creating opportunities to design nanoparticles with highly tunable properties. This study investigates the influence of channel geometry, flow parameters, and polymer concentration on the size and polydispersity of poly(butylene oxide) nanoparticles. Poly(butylene oxide) is a model hydrophobic polymer that is prone to forming large nanoparticles in bulk nanoprecipitation (typically >176 nm) and large aggregates with particle sizes ranging from 3000 to 5000 nm. Using a hydrodynamic flow-focusing geometry (Ψ-geometry), we demonstrated that high total flow enhances convective mixing, shortens mixing times, and produces smaller nanoparticles with narrower size distributions. Comparative evaluations of Ψ- and T-channel geometries with varying dimensions showed that Ψ-geometries consistently outperformed T-geometries, yielding smaller and more uniform nanoparticles due to superior mixing efficiency. Reducing channel dimensions (down to 20 µm) further improved mixing efficiency by shortening diffusion distances and accelerating solvent-water interdiffusion. Ψ-geometry enabled nanoparticle sizes as small as 66 nm, whereas T-geometry produced significantly larger particles (>500 nm). Optimization of flow parameters revealed that increasing the flow rate ratio of the aqueous to organic phase and reducing polymer concentration significantly decreased nanoparticle size. This work underscores the critical interplay between microfluidic geometry, channel dimensions, and flow conditions in tailoring nanoprecipitation processes for hydrophobic polymers like poly(butylene oxide). While challenges remain in scaling up production while maintaining precise control over nanoparticle characteristics, future directions include refining microfluidic chip designs, integrating temperature-controlled systems, and exploring novel chemistries. These advancements aim to expand the applicability of microfluidics in nanoparticle synthesis for advanced biomedical applications.

1. Introduction

Nanoprecipitation,[1] also known as solvent displacement, Ouzo effect, or flash precipitation, is a versatile method for producing nanoparticles,[1] liposomes, and nanoemulsions.[2] For polymeric nanoparticles, this process involves mixing two immiscible phases: an organic phase and an aqueous phase. The organic phase comprises a solvent in which the polymer is dissolved. The aqueous phase comprises water, which is a non-solvent of the polymer. Surfactants could be added to each phase to increase nanoparticle suspension stability. A drug could be added to the organic phase for designing drug-loaded nanoparticles. Water-miscible organic solvents are typically acetone, ethanol, tetrahydrofuran, or acetonitrile. The miscibility of the organic solvent with water is required and represents a critical parameter for nanoprecipitation.[2]

In bulk nanoprecipitation (Fig. 1.a), the organic phase is introduced into an aqueous phase under constant stirring. As the water-miscible solvent diffuses into the aqueous phase, the polymer solubility decreases, inducing nanoparticle nucleation followed by aggregation.[3] The method of introducing the organic phase to the aqueous phase varies in the literature, with approaches including rapid mixing via syringe, dropwise addition, or using a funnel. These variations can significantly affect the mixing dynamics and, consequently, the properties of the resulting nanoparticles. In particular, controlling nanoparticle size is a critical factor for many applications, particularly in the biomedical field, where nanoparticles are used as drug delivery systems. Small nanoparticles (typically < 100 nm) are highly desirable because they exhibit improved cellular uptake, enhanced tissue penetration, and prolonged circulation times compared to larger particles. In addition, small nanoparticles are less likely to be recognized and cleared by the mononuclear phagocyte system, allowing for better biodistribution and drug delivery efficiency. The ability to precisely control nanoparticle size is also essential for optimizing drug loading and release profiles.

[a.] *Chimie ParisTech, PSL University, CNRS, Institut de Recherche de Chimie Paris, 75005 Paris, France.*
[b.] *Monash University, Clayton, Australia.*
[c] *Gulliver, CNRS, ESPCI Paris, Université PSL, 75005 Paris, France*
[d] *Sorbonne Université, CNRS, Institut Parisien de Chimie Moléculaire, IPCM, F-75005 Paris, France*
[e] *Institut Pierre Gilles de Gennes (IPGG), ESPCI Paris, Université PSL, 75005 Paris, France*
[#] Equally contributing first authors
* Corresponding authors
Supplementary Information available: [details of any supplementary information available should be included here]. See DOI: 10.1039/x0xx00000x

In bulk nanoprecipitation, key factors influencing nanoparticle size and characteristics include the solvent-to-water ratio, stirring speed, and the concentration of stabilizers or surfactants. However, bulk nanoprecipitation presents several limitations, including high polydispersity, large nanoparticle sizes, low batch-to-batch reproducibility, and challenges in scaling up. Maintaining consistent mixing conditions in large-scale production often proves difficult, leading to variability in nanoparticle properties and hindering their use in sensitive applications such as nanomedicine.

To address these limitations, researchers have explored various strategies to improve the mixing process. A notable advance was the introduction of a pilot setup by Fessi's group, which utilized a T-mixer to blend the organic and aqueous phases, reducing nanoparticle size from 141 nm to 105 nm.[4] In another investigation, a Y-mixer with controlled internal diameters (0.8–4 mm) was designed to optimize nanoemulsion and nanoparticle size.[5, 6] Smaller internal diameters of the Y-mixer channel significantly reduced particle size, while other parameters, such as mixing temperature and total flow (*TF*), had a lesser impact.[5] Our findings also revealed power-law relationships between particle diameters, the Reynolds number (*Re*, characterizing the balance between viscous and inertial stresses, Eq. 1), and shear rates, highlighting the role of turbulence in reducing droplet size. However, even with these improvements, the smallest achieved droplet size was 185 nm for a Y-mixer with a 0.8 mm diameter and a *Re* of 12,000. Typically, the flow would be turbulent in those conditions.[7]

In this context, microfluidics offers an alternative to bulk nanoprecipitation. Microfluidics, which involves the precise manipulation of nanoliter volumes within microscale fluidic channels, enables rapid and tunable mixing. This technology facilitates the control of process parameters over nanoprecipitation, allowing for systematic variation of flow rates and mixing times on a single platform. Unlike bulk methods, microfluidics can achieve consistent particle sizes even under laminar flow conditions, which dominate microchannel flows due to low Reynolds numbers.[8] While laminar flow simplifies some aspects of operation, it poses challenges for mixing, as diffusion becomes the primary mechanism for phase interaction. To overcome these challenges, significant research has been dedicated to designing efficient micromixing schemes. Precise engineering of device geometries has enabled enhanced control over mixing speed and efficiency, with mixing times (τ_{mix}, the time required for complete mixing) in straight rectangular channels calculated according to Eq.2.

Despite progress in microfluidic-assisted nanoprecipitation, most research focused on flow-focusing geometry devices (Fig. 1.b), with limited attention given to the impact of microfluidic channel geometry and dimensions on nanoparticle size. This study builds on the hypothesis that nanoparticle size and polydispersity can be reduced by increasing the speed of mixing between the two phases (u_{mix}) calculated according to Eq.3 and consequently by increasing the total flow.

In this investigation, we selected poly(butylene oxide) (PBO) as a model hydrophobic polymer since the design of nanoparticles composed of PBO by nanoprecipitation is yet to be reported. Indeed, PBO is usually linked to a hydrophilic block of poly(ethylene oxide) to obtain polymeric micelles.[9] Hydrophobic polymers led to a higher loading of hydrophobic drugs and a slower drug release than amphiphilic polymers.[10] However, nanoprecipitation of hydrophobic polymers leads to larger nanoparticles.[10] We first synthesized and characterized PBO, followed by nanoparticle design in bulk nanoprecipitation. Then, we designed PBO nanoparticles in a microfluidic device. From this perspective, we evaluated the impact of microfluidic cross-sections, total flow, flow ratio, microfluidic geometry, and the presence of mixing junctions on nanoparticle size (Fig. 1.c,d). The impact of the presence of a junction with dimensions smaller than the total flow and flow ratios aimed to further increase the speed of mixing of the two phases and to understand its impact on nanoparticle size. For each parameter, we calculated mixing velocities and the Reynolds number to elucidate the underlying mechanisms governing particle size control. By establishing relationships between nanoparticle size and process parameters, such as total flow, the Reynolds number, and thus mixing speed, we aimed to provide a framework for achieving consistently smaller, monodisperse nanoparticles for advanced applications.

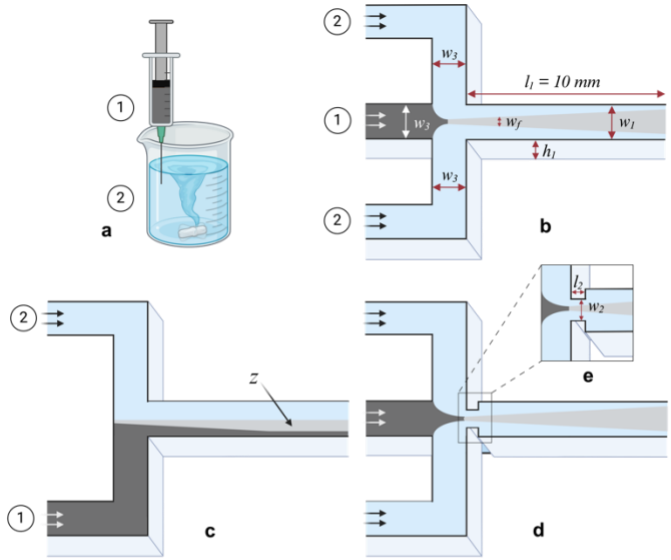

f

Chip channel dimensions for T, Ψ and Ψ_J-geometry			Dimensions of the junction for Ψ_J-geometry		
w_1 (μm)	h_1 (μm)	$A_{Channel}$ (10^2 μm²)	w_2 (μm)	l_2 (μm)	A_J (10^2 μm²)
100	100	100	20	30	20
40	40	16	8	12	-
20	20	4	4	8	0.8

Fig. 1: Schematic representation of bulk nanoprecipitation (a) and in a microfluidic-assisted device (b,c,d). Different geometries were used for microfluidic devices: Ψ-geometry without junction (b), T geometry (c), and Ψ_J-geometry with a junction (d). Dimensions of the channel chips and J-geometry junction (detailed in e) are indicated in (f). The channel length (l_1) and the channel width before mixing (w_3) were kept constant (l_1 = 10 mm and w_3 = 75 μm). (1) aqueous phase, (2) organic phase. The light grey region (*z*) represents the interdiffusion zone. A represents the cross sections of the channel ($A_{Channel}$) or the junction (A_J).

2. Results

2.1. PBO synthesis and characterization

PBO homopolymer was synthesized by anionic ring-opening polymerization using benzyl alcohol-*t*BuP$_4$ as the initiating system (**Scheme 1**). Benzyl alcohol hydroxyl groups were deprotonated by

*t*BuP$_4$ phosphazene base, generating extremely reactive alcoholates associated with phosphazenium cations, which initiated the polymerization of BO monomers (Fig. 2.a-c). The resulting PBO was passed through neutralized aluminum oxide. After this work-up, the ^{1}H NMR spectrum displays all the characteristic signals from both PBO and benzyl alcohol, and no phosphazenium traces were detectable on the ^{1}H NMR spectrum at 2.7 ppm (Fig. 2.b'). The experimental molar mass was determined by ^{1}H NMR ($M_{n(NMR)}$), comparing the signal integration of the initiator methylene group at 4.53 ppm with that of the methyl group in the repeating unit at 0.91 ppm. An M_n of 6100 g mol^{-1} was obtained, which is in very good agreement with the theoretical value ($M_{n(theo)}$ = 6400 g mol^{-1}). The PBO was then characterized by size-exclusion chromatography using PMMA standards. The resulting SEC trace is monomodal with a low dispersity of 1.07 (Fig. 2.d). $M_{n(SEC)}$ is slightly higher than $M_{n(theo)}$, but this difference can be attributed to the use of a PMMA standard.

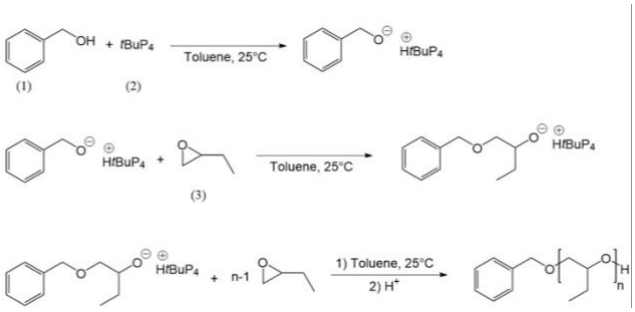

Scheme 1. Schematic representation of PBO polymerization. (1) corresponds to benzyl alcohol, (2) to phosphazene base *t*BuP4, and (3) to butylene oxide.

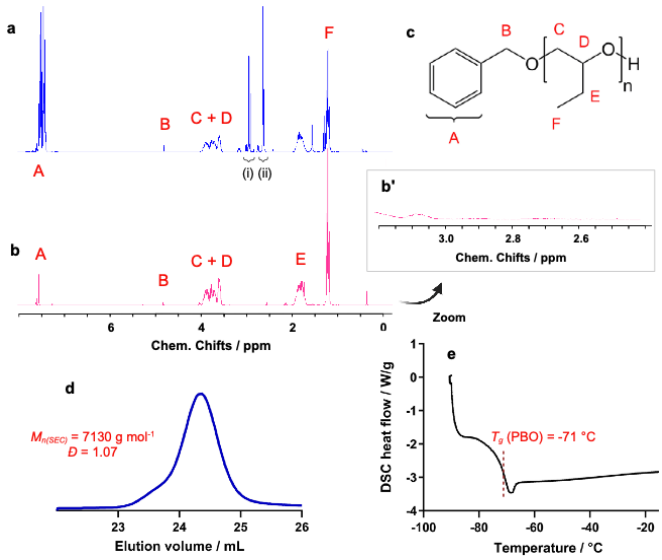

Fig. 2. Chemical characterization of PBO. NMR ^{1}H ($CHCl_3$d, 298 K, 300 MHz, 64 scans) of PBO before treatment with alumina (a) and after treatment with alumina (b). In (b') a magnification of (b) spectrum. The chemical structure of PBO and corresponding NMR peaks are given in (c). In (d) SEC (in tetrahydrofuran) of PBO (PMMA standard), and in (e) DSC of PBO showing a glass transition temperature (T_g) at -71 °C. $M_{n(theo)}$ = 6400 g mol^{-1}, $M_{n(NMR)}$ = 6100 g mol^{-1}, $M_{n(SEC)}$ = 7130 g mol^{-1}. The polydispersity index ($Đ$) determined by SEC was 1.07. The peaks in (i) and (ii) correspond to phosphazene and toluene, respectively.

DSC analysis indicates that the PBOs are amorphous, showing only a glass transition temperature (T_g) at -71 °C (Fig. 2.e), which is consistent with previously reported values.[11] The T_g of PBO being lower than room temperature and the polymer being atactic, thus lacking a crystalline melting point, results in PBO being in a liquid state at room temperature. This property is particularly relevant for applications requiring increased molecular mobility, such as film formation or the encapsulation of hydrophobic active ingredients into nanoparticles. The absence of crystallinity, combined with a low T_g, also enhances miscibility with other organic compounds, which can facilitate formulation processes and nanoprecipitation.

2.3. Design of PBO nanoparticles via bulk nanoprecipitation

Following the characterization of PBO's chemical properties, its apparent solubility was evaluated in ethanol and in water. PBO was found to be insoluble in water but soluble in ethanol at a concentration of 15 mg mL^{-1}. For nanoprecipitation, a working concentration of 7.5 mg mL^{-1} was selected, as this range (5–10 mg mL^{-1}) is known to produce small nanoparticles.[12] Furthermore, PBO was found to be insoluble in a 1:2 v/v ethanol/water mixture.

To achieve smaller nanoparticle sizes, the PBO molar mass was maintained below 10,000 g mol^{-1}, as higher molar masses of hydrophobic polymers are associated with larger nanoparticle sizes and increased aggregation.[12] Rapid mixing of the organic and aqueous phases was implemented to enhance solvent-water interdiffusion, which is crucial for reducing nanoparticle size. The organic phase was thus rapidly injected into the aqueous phase using a syringe rather than via dropwise addition to ensure optimal mixing conditions. Specifically, the injection of 1 mL of the organic phase was completed within 4 seconds, ensuring rapid and uniform dispersion.

Dynamic light scattering (DLS) analysis of the nanoparticle suspension revealed a heterogeneous size distribution ranging from 80 to 255 nm (Fig. 3a). The calculated *z*-average from three independent experiments was 176 ± 7 nm, with a polydispersity index (PDI) of 0.142, indicating relatively low polydispersity.

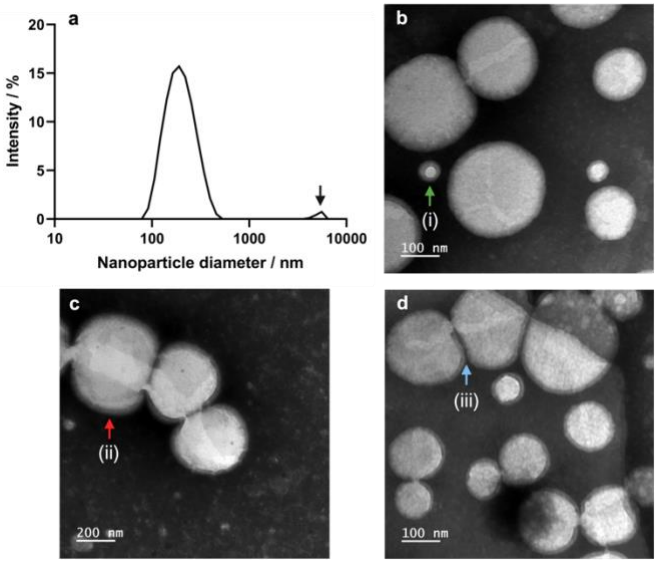

Fig. 3. Physicochemical characterization of PBO nanoparticles designed via bulk nanoprecipitation. The nanoparticle diameter in (a) was obtained by DLS. TEM images in (b), (c), and (d) were observed after adding a contrast agent. In (a), the black arrow corresponds to aggregates of PBO nanoparticles.

Transmission electron microscopy (TEM) images corroborated these results, showing nanoparticle sizes consistent with the DLS data (Fig. 3b-d). The smallest observed nanoparticle size was 60 nm, while the largest was 250 nm (indicated by green and red arrows in Fig. 3b

and Fig. 3c, respectively). However, some particles appeared to be adhered together or deformed (blue arrow in Fig. 3d). This aggregation could account for the appearance of a secondary population in the DLS analysis, with particle sizes ranging from 3000 to 5000 nm (black arrow in Fig. 3a). The heterogeneous nanoparticle size and aggregation are likely consequences of the mixing conditions inherent to bulk nanoprecipitation. Even though the organic phase was rapidly injected into the aqueous phase, the continuously changing volume ratio and flow rate between the two phases during mixing likely contributed to size variability and aggregation. As detailed in the next session, future studies may need to refine these mixing parameters to improve size homogeneity by microfluidic-assisted nanoprecipitation.

2.3. Design of PBO nanoparticles via microfluidic-assisted nanoprecipitation in hydrodynamic flow focusing (Ψ-geometry)

We employed a Ψ-geometry, flow-focusing microfluidic device with channel dimensions maintained at 100 × 100 μm to design PBO nanoparticles. The flow ratio was maintained at 0.06, corresponding to an organic-to-aqueous phase ratio of 1:15, as lower flow ratio values are known to produce smaller nanoparticles.[10] Four trials were conducted with a constant flow ratio of 0.06 and PBO polymer concentrations of 15, 7.5, 3.75, and 1.87 mg mL^{-1}. For each trial, the total flow was systematically increased from 32 to 96 μL min^{-1}, a threefold range.

The results presented in Fig. 4a and 4b show a clear relationship between polymer concentration and nanoparticle characteristics. Decreasing the polymer concentration consistently reduced the mean hydrodynamic diameters and PDI of the nanoparticles, demonstrating a significant effect of polymer concentration on nanoparticle size regardless of the total flow (Fig. 4a(i) and 4b(iv)). These observations highlight the critical role of polymer concentration in determining nanoparticle size under microfluidic conditions.

Polymer concentration influences the balance between nucleation and growth during nanoprecipitation. At higher concentrations (*e.g.*, 15 mg mL^{-1}), the abundance of polymer chains in the organic phase increases the likelihood of aggregation, resulting in larger nanoparticles. In contrast, lower polymer concentrations limit the aggregation step, producing thus smaller and more uniform nanoparticles. This trend was consistent across all tested total flow values, confirming that polymer concentration plays a dominant role in nanoparticle size regulation.

The impact of total flow on nanoparticle size was assessed for each polymer concentration (Fig. 4a(ii)). Statistical analyses revealed no significant differences in nanoparticle diameter upon varying total flow for a given concentration. A similar observation was made for PDI variation in Fig. 4b(v). While total flow influences mixing speed, the results suggest that within the tested range, the mixing conditions were sufficient to ensure efficient solvent-water interdiffusion for each concentration.

To further investigate the effect of polymer concentration, nanoparticle size was analyzed at fixed total flow values (Fig. 4a(iii)). The results demonstrated a significant size reduction with decreasing PBO concentration. For instance, at a total flow of 32 μL min^{-1}, nanoparticle size decreased from 593 nm for 15 mg mL^{-1} to 173 nm for 1.87 mg mL^{-1} PBO concentration. These findings reinforce the critical influence of PBO polymer concentration on nanoparticle size under microfluidic conditions.

At high PBO concentrations (15 mg mL^{-1}), the large nanoparticle sizes observed are unlikely due to aggregation, as no signals corresponding to particles larger than 600 nm were detected in DLS measurements (Fig. 4c). Instead, the broad PDI observed at low total flows (32 and 64 μL min^{-1}) may be attributed to the emergence of a secondary population of smaller nanoparticles. This secondary population was absent at higher total flows (96 μL min^{-1}), where rapid mixing between the organic and aqueous phases likely suppressed secondary nucleation and aggregation. Notably, the mixing speed (u_{mix}) reached 160 mm s^{-1} at 96 μL min^{-1}, as detailed in Table S1 in the Supporting Information.

The results underline the interplay between polymer concentration and total flow. Higher polymer concentrations increase the availability of polymer chains, favoring larger particle formation and broader size distributions. However, the microfluidic platform allows for precise control of mixing, mitigating some of these effects at higher total flows. In this first optimization section, we demonstrated the feasibility of PBO nanoparticle design in a microfluidic device. For the next section, we investigated the impact of flow parameters on nanoparticle size and polydispersity. However, by decreasing the concentration of PBO from 15 mg mL^{-1} to 1.875 mg mL^{-1}, the mass of particles contained in the nanoparticle fraction further decreases by a factor of 8, massively lowering the mass yield of nanoparticles collected. For the next section, we optimized the flow parameters while keeping the PBO concentration constant at 3.75 mg mL^{-1} and the microfluidic geometry unchanged.

2.4. Effect of flow parameters on PBO nanoparticle size and polydispersity in hydrodynamic flow focusing (Ψ-geometry)

2.4.1. Impact of the flow rate ratio on PBO nanoparticle size

In this section, we first varied the flow ratio between the organic and the aqueous phases from 0.1, 0.08, 0.06, and 0.05, corresponding to the following ratios: 1:10, 1:12, 1:15, and 1:20. The first observation from the results of PBO nanoparticle size was measurements in Table S2 is that flow ratio variation significantly impacts the nanoparticle size during nanoprecipitation of PBO. A smaller flow ratio indicates a higher relative flow rate of the aqueous phase compared to the organic phase.

Small nanoparticles were obtained at low flow ratio values (0.05 and 0.06), corresponding to a high aqueous phase flow compared to organic flow (203-242 nm), as detailed in Table S2. The mixing time in those conditions was 2-3 ms (Table S2). At those low flow rate values, the aqueous phase dominates, leading to enhanced shearing of the organic stream at the interface. This results in rapid diffusion of the solvent into the aqueous phase and more efficient nucleation.

Large nanoparticles were obtained at high flow ratio values (0.1 and 0.08), corresponding to a higher organic phase flow compared to organic flow (306-380 nm) (Table S2). When the flow of the organic phases increases, the mixing time increases (2-7 ms), leading to less efficient mixing. Consequently, the diffusion of ethanol into the aqueous phase takes longer owing to the larger cross-section of the organic phase in the microfluidic chip.

ARTICLE

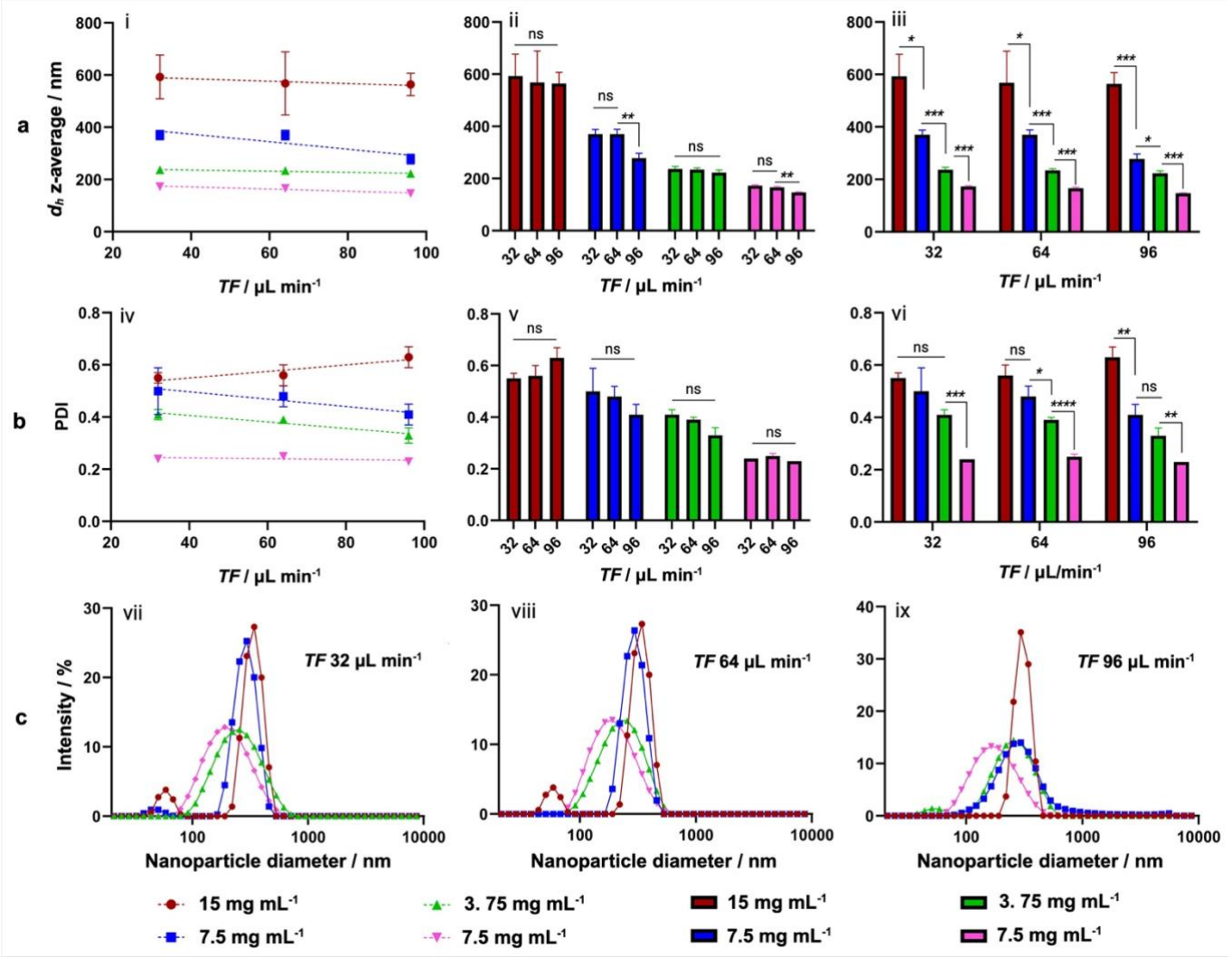

Fig. 4.Effect of PBO Concentration and total flow (*TF*) on Nanoparticle Size and PDI. (a) Mean hydrodynamic diameters (d_h) as a function of *TF*. (i) d_h values plotted on a consistent scale across *TF* values. (ii) Data presented to emphasize the effect of *TF* on d_h at each PBO concentration. (iii) Results plotted to highlight the effect of PBO concentration on d_h for each *TF* value. (b) Variations in PDI as a function of PBO concentration and *TF*. (iv) PDI values plotted versus *TF*. (v) Results highlighting the effect of *TF* on PDI at each PBO concentration. (vi) Data emphasizing the effect of PBO concentration on PDI at specific *TF* values. (c) Nanoparticle size distributions at *TF* values of 32 µL min^{-1} (vii), 64 µL min^{-1} (viii), and 96 µL min^{-1} (ix). PBO concentrations were 15 mg mL^{-1}, 7.5 mg mL^{-1}, 3.75 mg mL^{-1}, and 1.875 mg mL^{-1} at a flow ratio (*R*) of 0.06 (1:15). Statistical analysis was performed with two-way ANOVA followed by Tukey's post-test. One, two, three, and four asterisks denote a *p*-value < 0.05, < 0.01, < 0.001, and <0.0001, respectively. "ns" denote a non-significant difference. Data represent mean values from three independent experiments (n = 3).

Larger nanoparticles are thus formed as slower mixing favors growth processes over nucleation, allowing more PBO chains to coalesce into larger particles.

Those findings could be related to the Ψ-geometry corresponding to a microfluidic hydrodynamic flow-focusing setup, the organic phase is focused into a narrow stream by the surrounding aqueous phase in the microchannel. The mechanism of the influence of the flow ratio on particle size may be due to multiple factors. At a low flow ratio, the thin organic stream has a higher surface-to-volume ratio, favoring the interdiffusion of the species, reducing mixing time, and creating uniform, smaller PBO nanoparticles. At a high flow ratio, however, a thicker organic stream reduces surface area relative to volume, resulting in less efficient mixing and larger, more heterogeneous nanoparticles.

By decreasing the flow ratio, the hydrodynamic flow focusing stream becomes thinner, such that the width of the inner organic stream is decreased, as exhibited in Fig. 5c and 5d. Therefore, a smaller volume of nucleating particles would be present in the mixing chamber at any given time compared to high flow ratio values. This could lead to a lower proportion of colliding particles being present, thus resulting in less aggregation and a smaller average nanoparticle diameter.

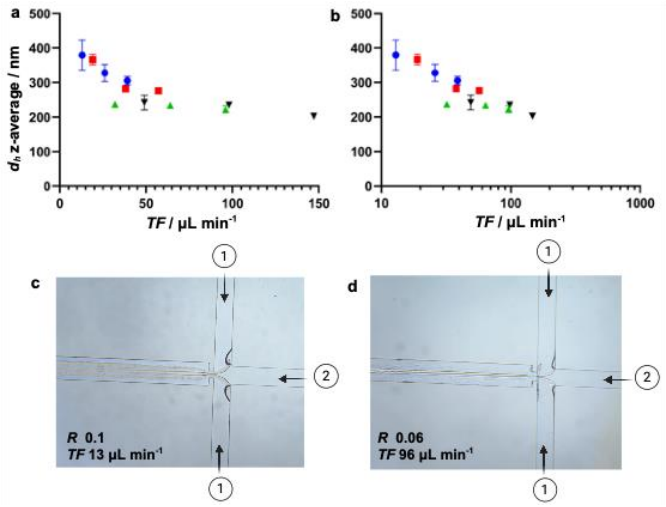

Fig. 5. Effect of total flow (*TF*) and flow ratio (*R*) on nanoparticle mean hydrodynamic diameters (d_h) for Ψ-geometry without junction. Nanoparticle size was plotted versus *TF* with a linear (a) and a logarithmic scale (b). *R* was changed as 0.1 (blue ●), 0.08 (red ■), 0.06 (green ▼), and 0.05 (black ▲), and the *TF* varies from 13 to 147 µL min^{-1}. (1) aqueous phase, (2) organic phase. Channel length l_1 was maintained at 10 mm. The PBO concentration was maintained at 3.75 mg mL^{-1}. Channels dimensions before mixing were w_3 = 75 µm and $h_{1\text{-}100}$ = 100 µm. Channels cross sections before mixing were $A_{B\text{-}100}$ = 7.5 × 10^3 µm^2. Channel dimensions after mixing were $W_{1\text{-}100}$ = 100 µm. Channel cross sections after mixing $A_{A\text{-}100}$ = 10^4 µm^2. (n = 3)

2.4.1. Impact of the total flow rate on PBO nanoparticle size

In a second set of experiments, the total flow rate was modified for each flow rate ratio. Regardless of the flow rate ratio, increasing the total flow rate decreased PBO nanoparticle size (Table S2 in the Supporting Data) and Fig. 5a. At low total flow, mixing of the two phases is diffusion-limited, leading to slower solvent-water interdiffusion. Longer mixing times allow PBO polymer chains to aggregate, resulting in larger nanoparticles. When total flow increases, the relative velocity between the two phases increases, appearing to accelerate the mixing kinetics. Smaller nanoparticles are thus formed as rapid interdiffusion promotes nucleation over growth. This was true for all flow rate ratios, as shown in Table S2 and Fig. 5a; even while less pronounced at the lowest flow ratio as in Fig. 4, the observation is well-pronounced at the larger flow ratio in Fig 5.

Quantitatively, the data displayed in Fig. 4a,b are seen to be monotonically decreasing with a smaller decrease at higher total flow. We thus characterize the data with a power law of the form $d_h = A(TF)^{-\alpha}$, with the least-squares regression shown in Fig. S1. The best-fitting values are $A = 800 \pm 300$ nm $\left(\text{min}\,\mu\text{L}^{-1}\right)^{\alpha}$ and $\alpha = 0.3 \pm 0.1$. The errors account for a 95% confidence interval. As discussed next, total flow is proportional to other relevant flow parameters, which could be similarly characterized with the power law above or other monotonically decreasing functions. Future work will be devoted to predicting the specific functional form of the observed decrease.

Variations of total flow directly impact the average flow velocity in the microfluidic channel (u_{mix} Eq.3). Besides, the velocity and the Reynolds number are directly proportional. Thus, an increase in total flow directly increases these two parameters. Conversely, the total flow is inversely proportional to the residence time (τ_{Res} Eq.4), and the latter also proportional to the mixing distance (L_{mix} Eq.5). These parameters are thus interdependent. Total flow affects the *Re*, which may, in turn, be correlated to the mixing dynamics, interdiffusion efficiency, and, ultimately, the PBO nanoparticle size. This dependence on the Reynolds number was especially noted in our previous studies for large Re in the turbulent regime; however, given the relatively small values encountered here (Table S4), we expect laminar flow.

Given the laminarity of the microflows employed here, the mixing is diffusion-limited. This relatively slow solvent-water interdiffusion can result in larger nanoparticles due to extended particle growth times and possibly aggregation. As total flow increases, the velocity increases, leading to higher Reynolds number values. Although turbulent flow is unlikely in our microchannels,[7] advection-diffusion coupling along flow stream lines may play a role in the phase separation dynamics and interfacial contact that lead to the formation of nanoparticles. Whatever the mechanism, the resulting solvent-water interdiffusion at high total flow yields smaller, more uniform nanoparticles. Enhanced convective mixing reduces the mixing time,

favoring nucleation over growth, leading to smaller, more uniform nanoparticles.

By increasing the total flow, the residence time of PBO nanoparticles in the microfluidic channel is decreased (Table S2). However, excessive total flow can lead to short residence times that are smaller than the time it takes a molecule (i.e. from the aqueous or organic phases) to cross the dispersant, potentially limiting polymer precipitation and affecting nanoparticle uniformity. Karnik et al.[10] found that for small-diameter, homogeneous nanoparticles, the residence time should be greater than τ_{mix} but less than the total aggregation time. Therefore, the sharp decreases in particle diameter observed in Fig. 5a may be due to mixing time becoming less than the total aggregation time, and the diameter then plateaus because the extent of aggregation has stabilized.[10] Increasing the total flow was not observed to have a significant effect on the PDI of the resulting nanoparticle suspension.

For the next section, to understand the impact of total flow and channel geometry on PBO nanoparticle size, we kept the flow ratio constant (R = 0.06) while modifying total flow, microfluidic geometry, and dimensions. In this way, the different velocities are obtained for the same R.

2.5. Effect of channel dimensions and geometry on PBO nanoparticle size and PDI

In microfluidic-assisted nanoprecipitation, hydrodynamic flow-focusing (Ψ-geometry) is the most commonly reported mixing strategy, while T-mixing—initially used for optimizing nanoprecipitation parameters—has been less frequently investigated. To evaluate the influence of channel geometry on nanoparticle size and polydispersity index (PDI), we first modified the device design from Ψ-geometry to T-geometry. For each geometry, we systematically varied the channel dimensions and recorded the results, as summarized in Fig. 6 and Table S3.

In T-geometry, the organic and aqueous phases are introduced from opposite sides of the channel and intersect at the mixing junction. Here, nanoparticle formation depends on the diffusion of solute molecules across the interdiffusion zone at the mixing point (denoted as "z" in Fig. 1c).[13, 14]

For the largest channel dimension (100 × 100 µm), the resulting nanoparticles were consistently larger (>350 nm) as compared to similar total flow in the Ψ-geometries, and regardless of the total flow rate (Fig. 6a, Table S3). The limited efficiency of molecular diffusion and heterogeneous local mixing conditions likely contributed to the larger nanoparticle sizes and broader size distribution.

Decreasing the channel size from 100 µm to 40 µm did not yield a significant reduction in nanoparticle size or PDI (Fig. 6, Fig. S2a, and Table S2). Larger PDIs observed in these channels may be attributed to inconsistent local mixing, resulting in uneven nucleation and growth dynamics.

For the smallest channels (20 µm), nanoparticle sizes decreased significantly (188–202 nm) at low flow rates (2–4 µL min^{-1}) and low Reynolds numbers (Re = 10–21). At these scales, laminar flow dominates, making molecular diffusion the primary mixing mechanism. The reduced diffusion distance between phases enhanced solvent-water interdiffusion, promoting smaller nanoparticle formation. However, operating at high flow rates in such small channels was challenging, and achieving optimal flow rates to balance nucleation and growth dynamics is essential for size uniformity.

In Ψ-geometry, the organic phase flows through a central channel and is symmetrically compressed by the aqueous phase from two lateral channels, creating a narrowly focused stream. This design optimizes nanoparticle formation through:

The focused organic stream minimizes diffusion distances, allowing rapid and efficient solvent-water interdiffusion. In particular, and for identical total flow and R, the presence of a wall in the T-geometry effectively halves the surface to volume ratio between the aqueous and organic phases. Furthermore, given the square channel cross sections used here, the hydrodynamic context of the T- and Ψ-geometries are distinct such that any influence of shear will be modified between them. Based on our observations, we hypothesize that these differing contexts promote uniform nucleation in the Ψ-geometry and limit particle growth, leading to smaller nanoparticles with narrower size distributions. The geometry facilitates rapid mixing at high speeds, displacing the organic solvent effectively, which is crucial for forming small and uniform nanoparticles. The symmetrical compression ensures consistent hydrodynamic focusing, minimizing mixing heterogeneity and resulting in lower PDIs. Experimental results confirmed that Ψ-geometry consistently produced smaller nanoparticles with narrower size distributions compared to T-geometry, particularly at high flow rates. This is attributed to the improved mixing efficiency and controlled nucleation environment provided by hydrodynamic focusing.

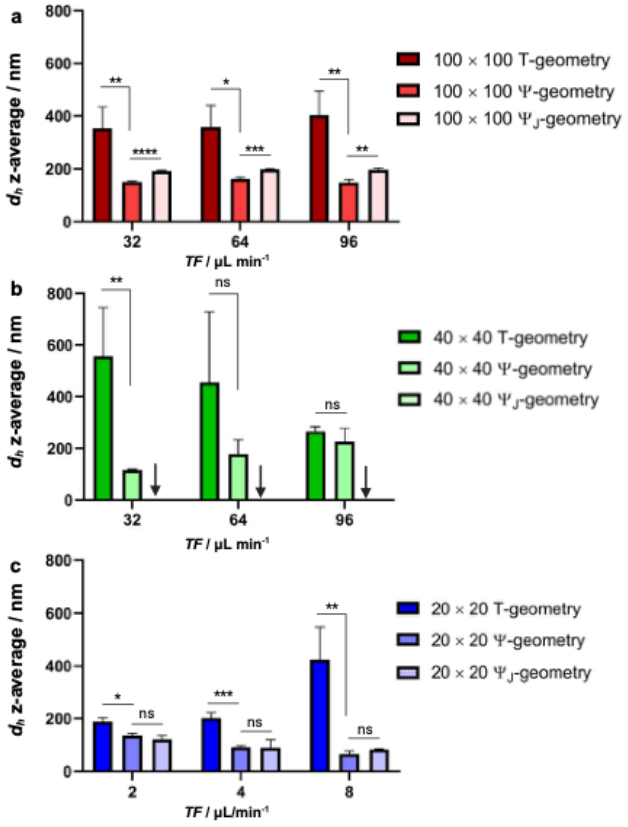

Fig. 6. Effect of channel geometry and total flow (*TF*) on mean hydrodynamic size of PBO nanoparticles. The flow ratio R was maintained at 0.06. The PBO concentration was 1.875 mg mL^{-1}. Statistical analysis was performed with two-way ANOVA followed by Tukey's post-test. One, two, three, and four asterisks denote a p-value < 0.05, < 0.01, < 0.001, and <0.0001, respectively. "ns" denote a non-significant difference.

To sum up this section, the results highlight the importance of precise channel design and optimization in achieving the desired nanoparticle size and uniformity. While T-geometry offers some control, it lacks the performance of Ψ-geometry for reducing nanoparticle size and PDI. The smallest PBO nanoparticle size (66 nm) was obtained by this geometry by using a 20 µm channel dimension. Additionally, simply introducing a mixing junction or reducing channel dimensions is insufficient for achieving significant improvements in nanoparticle size and polydispersity (Fig. 6 and Table S4).

3. Experimental section

3.1. Materials

Benzyl alcohol (BA, anhydrous, 99.8%, (1) in Scheme 1), phosphazene base *t*BuP$_4$ (1-tert-butyl-4,4,4-tris(dimethylamino)-2,2-bis[tris(dimethylamino)-phosphoranylidenamino] 2λ5,4λ5-catena di(phosphazene)) (0.8 mol L^{-1} in n-hexane, (2) in **Scheme 1**), aluminum oxide, *N*,*N*-dimethylformamide (DMF), butylene oxide (BO, (3) in **Scheme 1**, HCl, $NaHCO_3$, calcium hydride (CaH_2, ca. 93%), deuterated chloroform ($CDCl_3$) and dimethyl sulfoxide (DMSO-d_6), surfactants (Tween® 80, Span® 80), and phosphotungstic acid (contrast agent for TEM observations) were purchased from Sigma-Aldrich (St. Quentin Fallavier, France). Lithium bromide (LiBr), dichloromethane (DCM), methanol, tetrahydrofuran, ethanol (>99.5%), and toluene were purchased from VWR Chemical (Pessac, France).

Noteworthy, BA and *t*BuP$_4$ were stored in a glovebox until use. The monomer BO was dried twice over calcium hydride by cryo-distillation and was then stored in a glovebox. A solvent purification system (MBraun SPS-800, Garching, Germany) was used to dry toluene and THF under nitrogen.

Polytetrafluoroethylene (PTFE) filters with a porosity of 0.22 µm were purchased from Merck (Guyancourt, France). Size exclusion chromatography (SEC) columns and poly(methyl methacrylate) standards were purchased from Polymer Standard Services (Agilent Technologies, Les Ulis, France). The glove box (MBraun Labstar, Garching, Germany) has a purification system and a dry nitrogen atmosphere.

Milli-Q® water was used for all the experiments (Resistivity 18.2 MΩ.cm at 21 °C, Millipore purification system, Millex, SLAP 0225, Millipore, France). Ethanol and water were filtered through a 0.45 µm filter before use.

The density and the viscosity of the aqueous and the organic as well as PBO nanoparticle suspension were determined as detailed in the Supporting Information (Table S5, S6 and Fig. S3).

3.2. Methods

3.2.1. PBO synthesis and characterization

3.2.1.1. PBO Synthesis. The PBO was synthesized in the glovebox according to the procedure reported by Illy et al.[15] Typically, BO (957 µL, 11 mmol, 87 eq.) was introduced into a 100 mL single-chambered glass flask (Lenz Laborglasinstrumente™ 03002970). Then, 1mL of toluene was introduced under nitrogen, followed by BA (13 µL, 0.126 mmol, 1 eq.), and *t*BuP$_4$ solution (125 µL, 0.1 mmol, 1 eq.). Notably, *t*BuP$_4$ and BA were added using a microsyringe (Hamilton Company, reference 87930), while toluene (1 mL) was added using a plastic syringe (B. Braun, reference 720-2561). After closure of the flask, the reaction was left under stirring at 25 °C for 24 h. An aliquot was collected from the polymerization tube and analyzed by ^{1}H NMR. The monomer peaks at 2.7 ppm were carefully examined. A complete conversion of the monomer corresponds to the , with the disappearance of the triplet at 2.7 ppm assigned to the monomer's epoxide ring. After confirming the consumption of BO, a termination step was undergone by breaking the inert conditions. Subsequently, the solvent was removed by rotary evaporation. Then, the polymer was dissolved in DCM and purified by passing through neutral aluminum oxide to eliminate *t*BuP$_4$. ^{1}H NMR in deuterated $CDCl_3$ confirmed the effectiveness of the purification. The solvent was removed by rotary evaporation under a vacuum at 50 °C, followed by drying overnight under vacuum to give a yellowish liquid.

3.2.1.2. PBO characterization. PBO number-average molar mass was determined by ^{1}H NMR spectroscopy (denoted $M_{n(NMR)}$). PBO ^{1}H NMR spectra were recorded in $CDCl_3$ using a Bruker 300 MHz NMR spectrometer. The polymer concentration in the solution was 15 mg mL^{-1}.

Size exclusion chromatography (SEC) in THF was carried out on three PL gel Mixed-C 5 µm columns (7.5 ´ 300 mm; separation limits: 0.2 to 2 × 10^6 g mol^{-1}) maintained at 40 °C and coupled with a Viscotek GPCmax delivery module and two modular detectors: a Viscoteck 3580 differential refractive index detector and a Shimadzu SPD20-AV diode array UV detector. The mobile phase flow rate was 1.0 mL min^{-1}, and toluene was used as a flow rate marker. Samples were prepared by dissolving PBO in tetrahydrofuran at a 5 mg mL^{-1} concentration. After filtration through a 0.22 µm pore-size PTFE syringe filter, PBO solution was injected (50 µL). The OmniSEC 4.7 software was used for data acquisition and analysis in all cases. The number-average molar mass $M_{n(SEC)}$ and the dispersity $Đ$ of the polymers were calculated from poly(methyl methacrylate) standards using a differential refractive index detector.

PBO thermal behavior was evaluated by differential scanning calorimetry (DSC) using a TA DSC Q2000 device (Guyancourt, France) calibrated with an indium standard. The sample was placed in an aluminum capsule and initially cooled to -80 °C. Two cycles of heating (10 K min^{-1}) and cooling (10 K min^{-1}) were then applied in the temperature range of -80 to +130 °C. The samples' glass transition temperatures (T_g) were taken from the midpoint of the step in specific heat increments using the second heating cycle.

3.2.2. PBO nanoparticle preparation via bulk nanoprecipitation

Nanoprecipitation was performed to prepare PBO nanoparticles by adapting the protocol published by Bouchemal et al.[2] For nanoparticle preparation, the organic phase was prepared by weighting in a small vial PBO (7.5 mg) and Span® 80 (2 mg), used as a lipophilic surfactant. Then, ethanol (1 mL) was added to the vial.[2] The organic phase was homogenized by a magnetic stirring for a few minutes. The continuous phase was prepared by weighting in a small vial Tween® 80 (6.8 mg), used as a hydrophilic surfactant. Then, water (2 mL) was added to the vial, followed by magnetic stirring until complete surfactant dissolution. The organic phase was then

collected in a 2-mL plastic syringe (B Braun™ 4606027V) with an 18-G needle (Microlance 3) and then rapidly injected into the continuous phase under magnetic stirring (400 rpm at 25 °C) (Figure 1.a). The injection speed was 4 s for 1 mL of organic phase. The magnetic stirring is maintained for 30 min. The organic solvent was removed by evaporating overnight under a fume hood at room temperature.[2]

3.2.3. PBO nanoparticle preparation via microfluidic-assisted nanoprecipitation for

3.2.3.1. Microfluidic chip fabrication. A commercial polydimethylsiloxane elastomer (PDMS, Momentive RT 615 A & B) was utilized for chip fabrication. PDMS and the associated crosslinker were mixed in a 10:1 ratio and poured onto a lithography-etched aluminum mold containing the microfluidic design given in Fig. 1. The design was then placed in a vacuum chamber under vacuum until all air bubbles were removed, typically for one hour at room temperature. The design was then transferred to an oven at 70 ºC for 3 h, allowing the PDMS to solidify. The individual chips were then cut from the mold, placed into a plasma cleaner with a glass microscope slide, and exposed to oxygen plasma at 50 W for one minute. Once removed from the plasma chamber, the chip was pressed gently, with the design facing down, onto the glass slide to finalize the chip. Inlet and outlet holes were punched into the chip using a coring punch. During storage, scotch tape was placed over the chip to prevent exposure to dust.

3.2.3.2. Nanoparticle preparation by microfluidic-assisted nanoprecipitation. Two 11 Pico Plus Elite Pump Module syringe pumps (Harvard Apparatus, Courtaboeuf, France) were loaded with 10 mL 100 Series gastight Hamilton syringes (Harvard Apparatus, Courtaboeuf, France) filled with the aqueous and polymer/oil containing organic phases, respectively. The syringes were attached to 0.5 mm silicone tubing fitted with 23G stainless steel microfluidic adaptors. The organic phase was connected to the inner inlet of the PDMS chip, the aqueous phase was connected to the outer inlet, and the entire chip setup was placed under a B-190TBPL Microscope (Optika Italy). The syringe pumps were connected to a Pump Controller (Harvard Apparatus, Courtaboeuf, France), wherein the aqueous and organic phase flow rates were programmed to satisfy the experimental requirements, as exemplified in Table 1. The experiment was run for sufficient time to collect 100 µL of the nanoparticle suspension, which was collected into 5 × excess ultrapure water and analyzed immediately via DLS. The concentration of PBO in the organic phase was varied as 15, 7.5, 3.75, and 1.875 mg mL^{-1}. For each PBO concentration, the total flow varied from 32 to 86 µL min^{-1}, and the flow ratio was $R = 0.06$.

3.2.3.3. Investigation of the impact of process parameter variation on nanoparticle size. Microfluidic geometry and dimensions were modified, as detailed in Fig. 1. A microfluidic hydrodynamic flow focusing (HFF) device was first explored (denoted as Ψ-geometry, Fig. 1.b), and the results compared to T-geometry (Fig. 1.c). Then, the impact of the presence of a junction (J-type) on mixing behavior and nanoparticle size was explored (Fig. 1.a). The results were compared to nanoparticle size obtained without junction (Ψ-type) (Fig. 2.b) and T-type geometry (Fig. 2.c).

3.2.3.4. Equations to calculate microfluidic parameters

$$Re = \frac{uw_1}{\nu} \quad (Eq.1)$$

Where u is the jet velocity (m s^{-1}) and ν is the kinematic viscosity of the organic phase before mixing (m^2 s^{-1}); u can be estimated from Eq. 3.

$$\tau_{mix} \sim \frac{w_f^2}{4D} \approx \frac{w_1^2}{9D} \frac{1}{\left(1+\frac{1}{R}\right)^2} \quad (Eq.2)$$

Where D represents the diffusivity index of the solvent in water (for ethanol, $D = 1.22 \times 10^{-9}$ m^2 s^{-1}) and R is the flow ratio. It is calculated by dividing the flow of the organic phase (Q_{Org}) by the flow of the aqueous phase (Q_{Aq}). w_f is the width of the focused stream (m) (Fig. 1.b and 1.c), and w_1 is the microfluidic channel width (m).

$$u_{mix} = \frac{TF}{A_{Channel}} \quad (Eq.3)$$

Where TF is the total flow, and $A_{Channel}$ is the microfluidic channel cross section (Fig. 1.f).

$$\tau_{res} = \frac{l_1}{u} \quad (Eq.4)$$

τ_{res} the residence time of the suspensions in the channel of the microfluidic device (s).

$$l_{mix} = u\tau_{mix} \quad (Eq.5)$$

l_{mix} is the mixing distance corresponding to the distance required for complete mixing (m).

3.4. Nanoparticle physicochemical characterization

3.4.1. Dynamic light scattering. Nanoparticle mean hydrodynamic diameters (d_h) were measured by dynamic light scattering (DLS) using a Zetasizer Nanoseries. Bulk nanoprecipitation samples were prepared by diluting 2 µL of the sample in 1 mL water. Microfluidic samples were not diluted. Particle size was measured at 25 °C. The scattering angle was 173°. Each experiment was replicated three times on three independent formulations.

3.4.2. Zeta potential. The particle surface potentials were calculated from the electrophoretic mobility using an electrophoretic light-scattering technique (Zetasizer Nanoseries, Malvern Instruments, Ltd., UK). For sample preparation, 500 µL of each suspension was diluted with NaCl (1 mM) (500 µL). Dilution was optimized to reach an attenuation of 6. Then, 1 mL of each suspension was placed in a disposable folded capillary cell (DTS1070). Zeta potentials were measured at 25 °C.

3.4.3. TEM. TEM characterizations were performed at 80 kV transmission using a transmission electron microscope (JEOL 1400) coupled to TEM Domain Centre software. Samples were prepared as detailed in our previous publication.[16] Typically, 1 µL suspensions were diluted in water (49 µL) and manually homogenized. Then, 4 µL suspensions were placed on a plasma-treated carbon grid for 40 seconds The samples were further stained with 2% (w/v) phosphotungstic acid for 40 seconds. After 5 min of drying at room temperature, the grid was placed on a slide and inserted into the microscope for observation.

3.5. Softwares

All ^{1}H NMR spectra were analyzed with Bruker Topspin software and referenced to residual proton peaks of deuterated solvent.

3.6. Statistical analyses

GraphPad prism® version 9.0 software was used for statistical analyses. A two-way Kruskal-Wallis test was applied, followed by a Tukey's multiple comparison post-test. The significance level for all statistical analyses was set at a p-value < 0.05.

Conclusions

The microfluidic-assisted nanoprecipitation of hydrophobic polymers, such as PBO, offers a versatile and precise platform for designing nanoparticles with controlled size and uniformity. PBO's hydrophobicity and specific molecular characteristics demand careful optimization of process parameters to control particle size and polydispersity. Our study underscores the potential of microfluidic devices in overcoming these challenges. For PBO nanoprecipitation in flow-focusing Ψ-geometries, we noted that lower flow rate ratios (organic:aqueous phases) generally produced smaller, more uniform nanoparticles due to enhanced solvent-water interdiffusion and rapid nucleation. In contrast, higher *R* values led to larger and more heterogeneous nanoparticles owing to the longer diffusion times and by extending growth phases. We also revealed that optimized *TF* values are crucial for achieving efficient mixing and precise nanoparticle formation. Higher total flow values improved mixing efficiency while maintaining laminar flow (*i.e.*, low to moderate Reynolds number, *Re*), enabling consistent PBO nanoparticle synthesis. When the mixing geometry and channel dimensions were varied, we discovered that the Ψ-geometry demonstrated superior performance in producing small, uniform PBO nanoparticles through its confined flow focusing, compared to the T-geometry, which exhibited greater variability, likely due to enhanced surface-to-volume ratio in the former geometry or to distinct hydrodynamic contexts between the geometries. Reducing channel dimensions, particularly to 20 µm, significantly improved nanoparticle size by shortening diffusion distances and enhancing mixing. However, incorporating mixing junctions did not show improved size uniformity for the chips used here.

Future studies could focus on how PBO's hydrophobic nature interacts with various active ingredients during encapsulation, particularly for poorly water-soluble drugs, to optimize drug-loading efficiency and release profiles. Beyond PBO, the insights gained here could guide the nanoprecipitation of other hydrophobic polymers, broadening the applicability of microfluidic platforms to diverse materials and biomedical applications.

Author contributions

CT: writing – review & editing, funding acquisition, discussion
HK: Investigation and methodology for PBO synthesis and characterization and nanoparticle design in bulk nanoprecipitation.
JDM: conceptualization, supervision, writing – review & editing, methodology, funding acquisition, discussion
KB: conceptualization, project administration, supervision, investigation, writing - the first draft, writing – review & editing, methodology, funding acquisition, discussion, resources
LA: Methodology, formal analysis, discussion
MM: formal analysis, discussion
NI: Supervision of PBO synthesis and characterization, discussion
PG: Supervision of PBO synthesis and characterization, discussion
SHC: methodology and supervision for the preparation of microfluidic chips.

Conflicts of interest

There are no conflicts to declare.

Acknowledgments

Authors Kawthar Bouchemal, Nicolas Illy, and Philippe Guegan received funding from the ANR (ANR-21-CE09-0015). Author Kawthar Bouchemal received funding from the ANR (ANR-23-CE06-0019) and Chimie ParisTech, PSL University. Authors Kawthar Bouchemal, Christophe M. Thomas, and Joshua D. McGraw received funding from the Institut Pierre-Gilles de Gennes and PSL University. The present study has benefited from the core facilities of Imagerie-Gif, (http://www.i2bc.paris-saclay.fr), member of IBiSA (http://www.ibisa.net), supported by "France-Bioimaging" (ANR-10-INBS-04-01), and the Labex "Saclay Plant Science" (ANR-11-IDEX-0003-02), the Institut Pierre-Gilles de Gennes (Equipex ANR-10-EQPX-34 and Labex ANR-10-LABX- 31) and PSL Research University (Idex ANR-10-IDEX-0001-02). The experimental work of this study also benefited from the technical contribution of the joint service unit CNRS UAR 3750 at the IPGG. No funders had any role in the study's design and data collection, analysis, and interpretation, nor in manuscript writing.

Notes and references

1. H. Fessi, F. Puisieux, J. P. Devissaguet, N. Ammoury and S. Benita, *International journal of pharmaceutics*, 1989, **55**, R1-R4.
2. K. Bouchemal, S. Briançon, E. Perrier and H. Fessi, *International Journal of Pharmaceutics*, 2004, **280**, 241-251.
3. J. Aubry, F. Ganachaud, J.-P. Cohen Addad and B. Cabane, *Langmuir*, 2009, **25**, 1970-1979.
4. S. A. Galindo-Rodríguez, F. Puel, S. Briançon, E. Allémann, E. Doelker and H. Fessi, *European journal of pharmaceutical sciences*, 2005, **25**, 357-367.
5. K. Mitri, C. Vauthier, N. Huang, A. Menas, C. Ringard-Lefebvre, C. Anselmi, M. Stambouli, V. Rosilio, J. J. Vachon and K. Bouchemal, *Journal of Pharmaceutical Sciences*, 2012, **101**, 4240-4247.
6. M. Stumpo, C. Anselmi, C. Vauthier, K. Mitri, I. Hanno, N. Huang and K. Bouchemal, *International Journal of Pharmaceutics*, 2013, **454**, 678-685.
7. K. Avila, D. Moxey, A. De Lozar, M. Avila, D. Barkley and B. Hof, *Science*, 2011, **333**, 192-196.
8. T. M. Squires and S. R. Quake, *Reviews of Modern Physics*, 2005, **77**, 977-1026.
9. D. A. Chiappetta and A. Sosnik, *European Journal of Pharmaceutics and Biopharmaceutics*, 2007, **66**, 303-317.

10. R. Karnik, F. Gu, P. Basto, C. Cannizzaro, L. Dean, W. Kyei-Manu, R. Langer and O. C. Farokhzad, *Nano letters*, 2008, **8**, 2906-2912.
11. R. Wehr, J. Gaitzsch, D. Daubian, C. Fodor and W. Meier, *RSC advances*, 2020, **10**, 22701-22711.
12. P. Legrand, S. Lesieur, A. Bochot, R. Gref, W. Raatjes, G. Barratt and C. Vauthier, *International journal of pharmaceutics*, 2007, **344**, 33-43.
13. R. F. Ismagilov, A. D. Stroock, P. J. Kenis, G. Whitesides and H. A. Stone, *Applied Physics Letters*, 2000, **76**, 2376-2378.
14. A. E. Kamholz, B. H. Weigl, B. A. Finlayson and P. Yager, *Analytical chemistry*, 1999, **71**, 5340-5347.
15. N. Illy, V. Corcé, J. Zimbron, V. Molinié, M. Labourel, G. Tresset, J. Degrouard, M. Salmain and P. Guégan, *Macromolecular Chemistry and Physics*, 2019, **220**, 1900210.
16. R. Diaz-Salmeron, C. Cailleau, S. Denis, G. Ponchel and K. Bouchemal, *Journal of Controlled Release*, 2023, **356**, 434-447.